Interfacial Modification as a Route to Novel Bilayered Morphologies in Binary Block Copolymer/Homopolymer Blends

Jonathan H. Laurer,[†,‡] Steven D. Smith,[§] Jon Samseth,[∥] Kell Mortensen,[⊥] and Richard J. Spontak*[,†]

Departments of Materials Science & Engineering and Chemical Engineering, North Carolina State University, Raleigh, North Carolina 27695, Corporate Research Division, The Procter & Gamble Company, Cincinnati, Ohio 45239, Department of Physics, Institute for Energy Technology, N-2007 Kjeller, Norway, and Department of Condensed Matter Physics & Chemistry, Risø National Laboratory, DK-4000 Roskilde, Denmark

Received February 9, 1998; Revised Manuscript Received May 13, 1998

ABSTRACT: Addition of a relatively low-molecular-weight parent homopolymer to a lamellar AB diblock copolymer constitutes a reliable means by which to induce, in controllable fashion, transitions to other morphologies. In this study, we examine the effect of interfacial modification on such transitions in "extended" A(A/B)B copolymer/homopolymer blends in which (i) the A/B midblock fraction (relative to the copolymer molecular weight) is varied from 0.0 to 0.4 in 0.1 increments and (ii) the overall concentration of A ranges from 0.50 to 0.95. As this A/B fraction is increased at constant blend composition, the extent of homopolymer-induced lamellar swelling becomes measurably less pronounced, indicating that the A/B midblock serves to delocalize repulsion along the interphase separating adjacent lamellae. At higher homopolymer concentrations, an increase in the A/B fraction results in the formation of either unilamellar vesicles or a randomly connected bilayered membrane, rather than micelles. These membranes become unstable and transform to micelles at high copolymer dilution. The results presented here are discussed in terms of the complex morphologies observed in, and predicted for, low-molar-mass (co)surfactant systems.

Introduction

Block copolymers remain a subject of extensive research interest due to their versatility in applications ranging from thermoplastic elastomers[1] to nanoscale templates[2] and switches,[3] as well as their fundamental ability to spontaneously self-organize into a variety of nanoscale microstructures. Microdomain ordering of block copolymers is generally driven by the thermodynamic incompatibility between the chemically dissimilar blocks.[4,5] For linear copolymers, this incompatibility is described by χN, where χ denotes the Flory−Huggins interaction parameter (expressed[5,6] in terms of entropic and enthalpic contributions as $\chi = \alpha + \beta/T$), and N is the number of statistical repeat units along the backbone. In addition, monomer asymmetry, monomer sequencing, and sequence length have also been identified as molecular characteristics governing the development of morphological characteristics and bulk properties in block copolymers.[7−10] Previous studies[11,12] designed to elucidate the impact of monomer sequencing on block copolymer morphological and property development have examined copolymers possessing tailored composition profiles along the backbone. An important example of a "tailored" copolymer is the *tapered* block copolymer, in which the composition varies continuously, rather than abruptly, from one block to the next. Chemical incorporation of a tapered A/B segment between the blocks of an AB diblock copolymer results in an increase in the free energy contribution of the interphase between microdomains due to enhanced mixing.[13] At sufficiently high fractions of the A/B midblock, the copolymer is ultimately driven toward its order−disorder transition (ODT), and weak-segregation behavior may be observed even for copolymers of large N.

Unfortunately, the composition profile along a tapered A/B segment is difficult to control from a synthetic standpoint. Moreover, isolation of the coupled effects arising from composition, monomer sequence, and sequence length constitutes a nontrivial task. This complication can be avoided through the use of model A(A/B)B copolymers, in which the A/B midblock is a random copolymer, exhibiting no systematic composition variation along the block.[14−16] A recent study[17] of compositionally symmetric (50/50 w/w A/B) A(A/B)B triblock copolymers in which the A and B units are styrene (S) and isoprene (I), respectively, has demonstrated that an increase in the S/I mass fraction ($w_{S/I}$), relative to the overall copolymer molecular weight, decreases the degree of copolymer segregation, as evidenced by a reduction in the microdomain period. Due to the corresponding increase in S and I mixing within the enlarged interphase between adjacent microdomains, we have designated such materials *extended* block copolymers (EBCs), although they have also been referred[18] to as ABC triblock terpolymers. As reported earlier,[19] the presence of a random S/I midblock in a S(S/I)I EBC may have a dramatic impact on the morphology of a blend composed of homopolystyrene (hS) and the EBC. At constant blend composition, for example, an increase in $w_{S/I}$ promotes bilayer, rather than micelle, formation. In this case, the random S/I midblock serves to (i) broaden the interphase between end block microdomains, thereby rigidifying the micro-

* To whom correspondence should be addressed.
† North Carolina State University.
‡ Present address: Department of Materials Science & Engineering, University of Pennsylvania, Philadelphia, PA 19104.
§ Procter & Gamble.
∥ Institute for Energy Technology.
⊥ Risø National Laboratory.

S0024-9297(98)00200-9 CCC: $15.00
Published on Web 07/10/1998

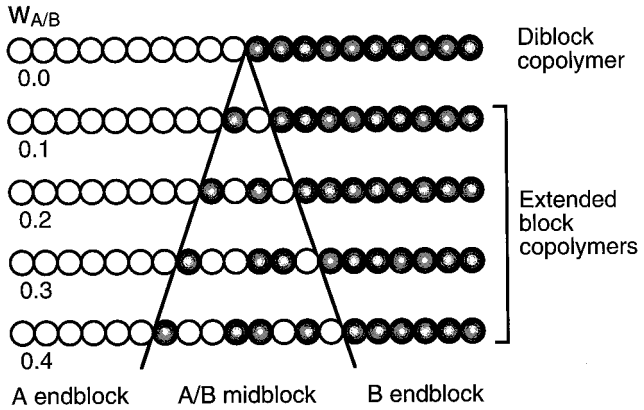

Figure 1. Illustration of the repeat unit sequencing in an AB diblock copolymer and four A(A/B)B extended block copolymers (EBCs) in which the A and B units are denoted by (○) and (●), respectively. As shown here, all the copolymers are compositionally symmetric, and the copolymer midblock fraction ($w_{A/B}$) is increased from 0.0 to 0.4 in 0.1 increments.

Table 1. Molecular and Microstructural Characteristics of the Block Copolymers Used in This Study

sample designation	$w_{S/I}$	w_S[a]	$\bar{M}_n$[b]	$\bar{M}_{S/I}$	M_S	R[c]	D[d] (nm)	D[e] (nm)
SI0	0.0	0.5	100 000	0	50 000	0.40	76.2	74.5
SI10	0.1	0.5	130 000	13 000	58 500	0.34	65.5	65.2
SI20	0.2	0.5	141 000	28 200	56 400	0.35	57.1	57.3
SI30	0.3	0.5	144 000	43 200	50 400	0.40	52.4	52.1
SI40	0.4	0.5	160 000	64 000	48 000	0.42	62.8	62.3

[a] Copolymer styrene weight fraction (from ^{1}H NMR). [b] Number-average copolymer molecular weight (from GPC). [c] Ratio of homopolystyrene molar mass to styrene block mass. [d] Lamellar period (±3%, from SANS). [e] Lamellar period (±7%, from TEM).

domain boundary with respect to curvature changes promoted by homopolymer addition; and (ii) reduce the extent to which the copolymer is microphase-segregated, which is anticipated to result in system disordering at reduced hS concentration. If $w_{S/I}$ is sufficiently large, random monomer sequencing along the EBC backbone may likewise affect local interactions with hS molecules.[8,16,20]

The purpose of the present study is to establish the blend conditions over which the effect of the S/I midblock in EBC/hS blends becomes morphologically significant. This objective is achieved through the use of a series of EBC copolymers in which $w_{S/I}$ is systematically varied in accord with the schematic illustration provided in Figure 1.

Experimental Section

Materials. One poly(styrene-*b*-isoprene) (SI) diblock copolymer ($w_{S/I} = 0.0$) and four poly[styrene-*b*-(styrene-*r*-isoprene)-*b*-isoprene] S(S/I)I copolymers with $0.1 \leq w_{S/I} \leq 0.4$ (in 0.1 increments) were synthesized via living anionic polymerization initiated by *sec*-butyllithium in cyclohexane at 60 °C. Each copolymer in this series is hereafter designated SI*m*, where *m* denotes the mass percent of the random S/I midblock. For the S(S/I)I copolymers, the randomness of the midblock was preserved (without tapering) through the use of a recently developed potassium alkoxide cocatalyst.[14−16] According to proton nuclear magnetic resonance (^{1}H NMR), all the copolymers were 50 wt % S. Table 1 reveals that the EBC molecular weight, as discerned from gel permeation chromatography (GPC), increases slightly as $w_{S/I}$ increases, while the lamellar period (D) from small-angle neutron scattering (SANS) generally decreases with increasing $w_{S/I}$.[17] [The styrene end block in each of these copolymers was 25% deuterated to provide scattering contrast.] Blends of each copolymer and a homopolystyrene (hS), also synthesized via living anionic polymerization, were prepared at several concentrations. Since the hS molecular weight was 20 000, the ratio of the molar mass of hS to that of the styrene end block of each copolymer (designated R) ranged from 0.34 to 0.42.

Methods. Films of EBC/hS blends with total styrene mass fractions (W_S) ranging from 0.70 to 0.95 were prepared from 4% (wt/v) toluene solutions cast into Teflon molds. Upon slow solvent evaporation over the course of 3 weeks, the resultant films, each measuring ca. 1 mm thick, were subjected to postannealing at 130 °C for 4 h under vacuum. Electron-transparent sections for transmission electron microscopy (TEM) were obtained through the use of a Reichert-Jung Ultracut-S cryoultramicrotome maintained at −100 °C. To enhance phase contrast, the isoprenic units were selectively stained by exposing the sections to the vapor of 2% OsO_4(aq) for 90 min. Cryofracture replicas of selected blends were also prepared by rapidly cooling small pieces of the annealed films to −170 °C in liquid ethane (cooled by liquid nitrogen) and subsequently fracturing the specimens under vacuum (ca. 10^{-6} Torr) in a JEOL JFD-9000C cryofracture-replication unit. Each fresh fracture surface was first shadowed with Pt−C at a 45° angle to produce topographic contrast and then coated with C deposited along the surface normal to ensure replica stability. Replicas were washed in toluene to remove all sample traces. Images of stained sections and cryofracture replicas were acquired on a Zeiss EM902 electron spectroscopic microscope operated at 80 kV and electron energy loss settings (ΔE) between 25 and 100 eV. At least 20 negatives were recorded from each blend composition, and representative images were selected for presentation. [Some blends were repeatedly prepared fresh, from the initial solution stage, to ensure reproducible microstructures.] Small-angle neutron scattering (SANS) was performed on the 2 MW reactor located at the Institute for Energy Technology in Kjeller, Norway. The neutron wavelength was 0.19 nm, and the sample-to-detector distance was maintained at 6.0 m. Two-dimensional scattering patterns were collected on a ^{3}He detector and corrected for detector efficiency and normalized with respect to water. One-dimensional patterns were then derived from azimuthal integration of the 2-D patterns. Microdomain periodicities (D) were ascertained from principal peak scattering positions (q^*) for blends exhibiting the lamellar morphology. According to Bragg's law, $D = 2\pi/q^*$, where the scattering vector (q) is given by $(4\pi/\lambda)\sin(\theta/2)$.

Results and Discussion

Conventional Diblock Copolymer Blends. Previous experimental studies of blends containing an ordered block copolymer and a parent homopolymer report that the molecular weight ratio of the homopolymer relative to that of the host copolymer block (R) constitutes an important consideration in ensuring homopolymer solubility within the compatible microdomains of the copolymer.[21−24] Generally speaking, $R < 0.5$ prevents macrophase separation between the homopolymer and ordered copolymer. Since $R = 0.38 \pm 0.04$ for the blends considered here, all the hS is expected to reside within the S microdomains of the SI diblock copolymer and the four S(S/I)I copolymers. Incorporation of homopolymer molecules into copolymer microdomains serves to alter the interfacial curvature of the microstructure.[25] Since the equilibrium morphologies for diblock copolymer/homopolymer blends are experimentally[25] and theoretically[26] established, confirmation of these morphologies in blends of the SI0 diblock copolymer with hS ensures that the blends have been properly prepared (i.e., all components were completely dissolved in a nonpreferential casting solvent, and the solvent evaporation rate was sufficiently slow to promote near equilibration of the microstructure). Such confirmation

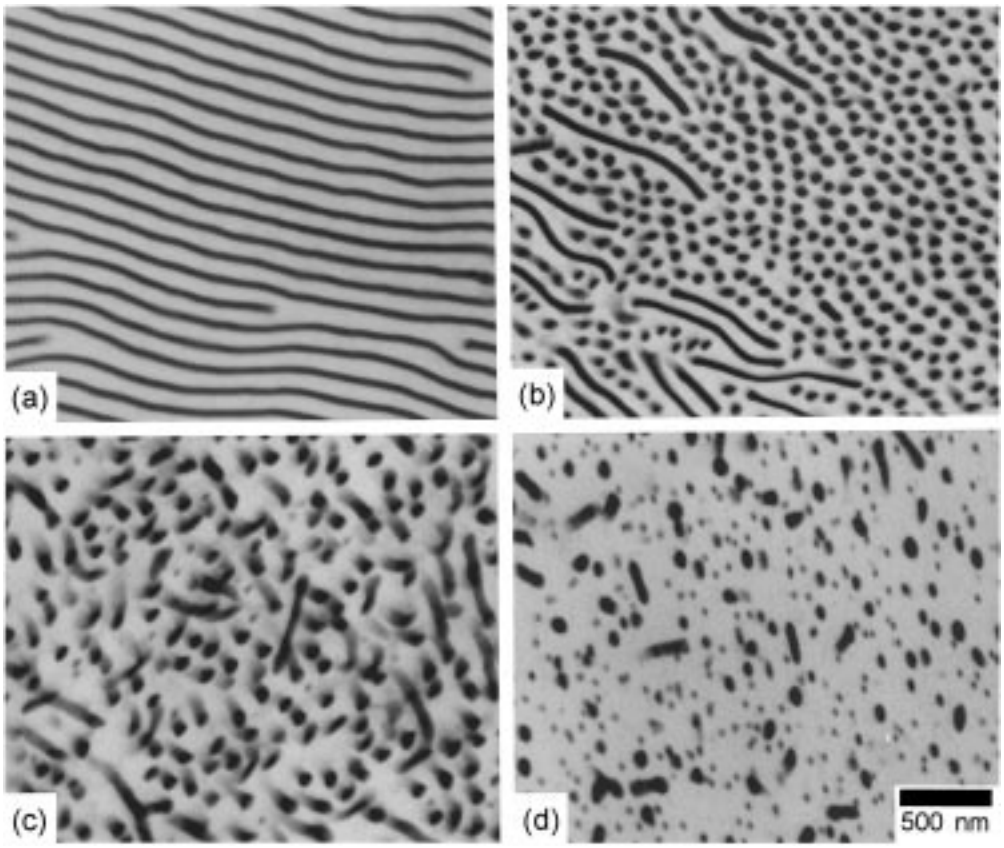

Figure 2. Series of TEM micrographs obtained from SI0/hS blends differing in overall styrene composition (W_S): 0.70 (a), 0.80 (b), 0.90 (c), and 0.95 (d). Transitions from alternating lamellae to dispersed isoprenic cylinders (a → b) and from cylinders to isoprenic micelles (c → d) are evident. Isoprene-rich microdomains appear electron-opaque (dark) due to selective OsO_4 staining.

is provided for the SI0/hS blends in Figure 2, in which several principal block copolymer morphologies are verified. The lamellar morphology, observed for the neat SI0 diblock copolymer, is retained in the blend with $W_S = 0.70$ (Figure 2a). Complete solubilization of hS within the lamellar S microdomains is inferred by noting the absence of macrophase-separated hS. The lamellar period of this blend is about 120 nm, representing a substantial increase (of about 60%) over the neat SI0 period (see Table 1) due to hS-induced swelling of the S-lamellae.[21,22,26−28]

Increasing the hS content results in morphological transitions from lamellae to isoprenic cylinders at $W_S = 0.80$ and $W_S = 0.90$ (Figure 2b,c, respectively), and ultimately to randomly arranged S micelles at $W_S = 0.95$ (Figure 2d). Measurements from micrographs such as those in Figure 2b,c reveal that the mean diameter of the isoprene cylinders ranges from 60 to 70 nm. A well-defined hexagonal lattice is not apparent in Figure 2b, but the cylinders appear reasonably well aligned throughout the sample (a conclusion drawn from TEM evaluation of several different microtomed sections in which cylinders aligned with their long axes nearly parallel to the electron beam appear as circles in projection). Although the cylinders in the SI0/hS blends with $W_S = 0.80$ (Figure 2b) and $W_S = 0.90$ (Figure 2c) possess comparable characteristic dimensions, the blend with $W_S = 0.80$ clearly exhibits greater long-range orientational order than the one with $W_S = 0.90$. No large grains of a single microdomain orientation are observed in the $W_S = 0.90$ blend.

A micellar morphology, consisting principally of dispersed spherical isoprene microdomains, forms in the blend with $W_S = 0.95$ (Figure 2d). The micelles evident in this image possess a surprisingly broad size distribution, since block copolymer micelles are typically relatively monodisperse.[29] We estimate that the average micelle diameter lies between 60 and 70 nm, in agreement with the diameters of the cylinders seen in Figure 2b,c. The lack of a bcc lattice in this and comparable images implies that, at this composition, this SI0/hS blend lies outside the ODT boundary.[5] Although the presence of a few rodlike microdomains suggests that further microstructural refinement may be possible in this specimen, the existence of spherical micelles possessing long-range order is not expected at this copolymer-dilute composition.[29] It can be concluded from Figure 2 that (i) the blends examined here have been given sufficient opportunity for the copolymer molecules to achieve stable (near-equilibrium) microstructures and (ii) the SI0/hS blends (in the absence of a random S/I midblock) exhibit morphologies that are expected from such blends.[22,25,26] Having addressed these preliminary issues, we now explore the effect of the random copolymer midblock on blend morphologies.

Extended Block Copolymer Blends. The lamellar morphology observed for the SI0/hS blend with $W_S = 0.70$ is also present in each of the EBC/hS blends at this composition, as shown in Figure 3 for the SI10/hS (Figure 3a) and SI20/hS (Figure 3b) blends. Since the neat copolymers all exhibit lamellae, it immediately follows that blends with $0.50 \leq W_S \leq 0.70$ must also possess lamellar, not bicontinuous,[24−26,30] microdomains. Analysis of a SI40/hS blend with $W_S = 0.60$ (data not shown) yields the lamellar morphology, which is consistent with this expectation. An increase in the styrene

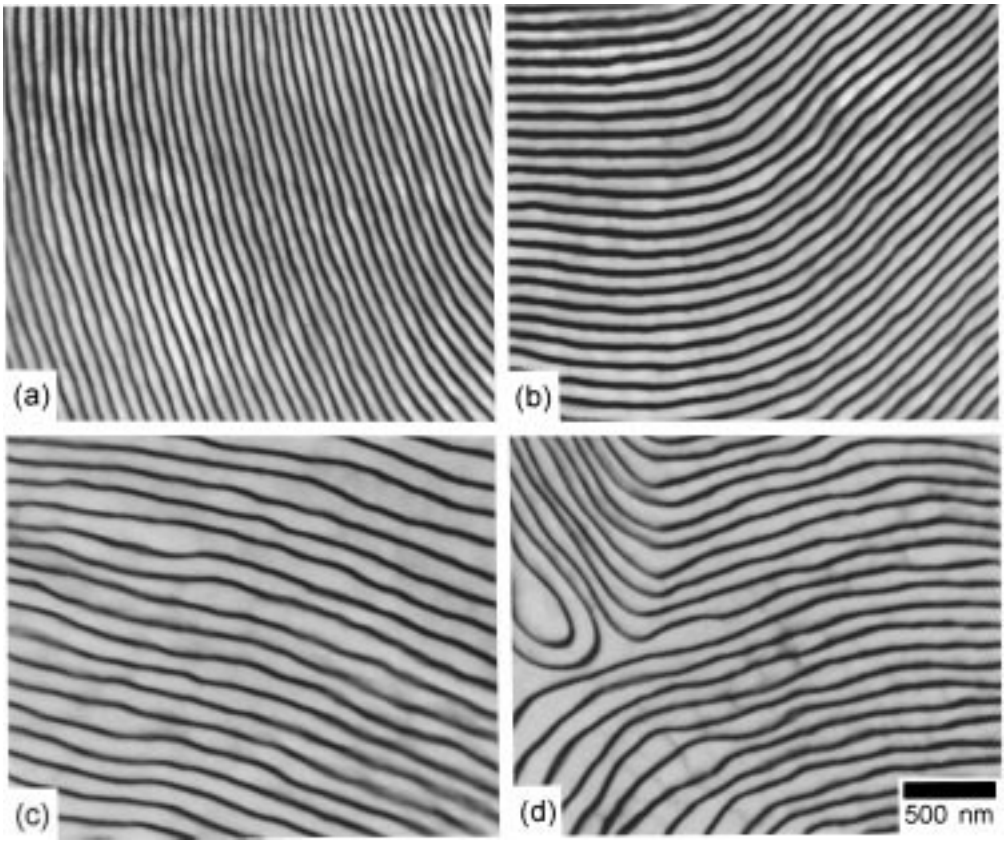

Figure 3. TEM micrographs of two lamellar EBC/hS blends at different W_S and $w_{S/I}$. The blends presented in (a) and (b) possess $W_S = 0.70$ and consist of EBCs with $w_{S/I}$ of 0.1 (SI10) and 0.2 (SI20), respectively. Blends evaluated at $W_S = 0.80$ are shown in (c) (SI10) and (d) (SI20). Since the corresponding SI0/hS blend at $W_S = 0.80$ exhibits the cylindrical morphology, the presence of a random midblock appears to broaden the lamellar stability regime at constant W_S.

content to $W_S = 0.80$, however, does not produce S cylinders in these EBC/hS blends as it had in the SI0/hS blend (Figure 2b). In fact, the SI10/hS and SI20/hS blends both exhibit a highly swollen lamellar microstructure at this composition (Figure 3c,d). It is evident from these micrographs that increasing W_S at a fixed midblock length results in a substantial increase in the interlamellar spacing due to the presence of homopolymer. Although the morphologies of the SI/hS and EBC/hS blends are similar in appearance, the interfacial chain packing of EBC molecules in the blends shown in Figure 3 differs from that of the SI molecules in the blends displayed in Figure 2. The presence of a random midblock increases conformational entropy in the interphase, since the location of the covalent junction point[31] between S and I end blocks is less restricted for an EBC molecule than for an analogous SI molecule. At a given temperature, the result of this enlarged interphase, schematically depicted in Figure 1, is an increase in the free energy of mixing (and a corresponding reduction in the extent of segregation) at a fixed blend composition. This effect, due entirely to the presence (and size) of the random midblock, has measurable consequences in the lamellar regime, since the effective interphase width is expected to increase with increasing $w_{S/I}$, thereby promoting reductions in both the microdomain cores and the microdomain period (D). Addition of hS to an EBC, on the other hand, is responsible for causing the S microdomain cores to swell.

The result of this competition between microdomain contraction and swelling has been examined by SANS performed on the lamellar blends. Results from this analysis are presented in Figure 4 for blends possessing $W_S = 0.70$. Each of the SANS profiles in Figure 4 exhibits a clear scattering maximum, resulting from interdomain interference. Separation of the Bragg planes in the lamellar morphology yields D from the peak position according to Bragg's law (see the Experimental Section). Values of D for each of the lamellar blends with $W_S = 0.70$ and 0.80, along with the values of the neat copolymers listed in Table 1, are displayed in Figure 5. In each case, measurements acquired from SANS correspond well to those estimated from TEM micrographs. Despite the variation in molecular weight

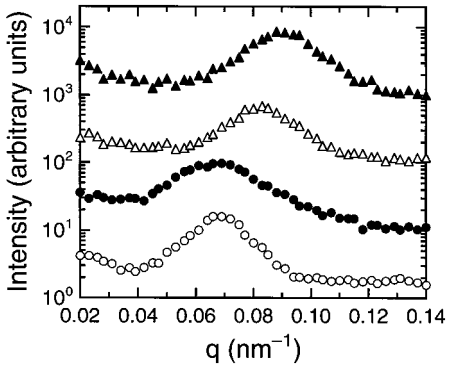

Figure 4. Small-angle neutron scattering (SANS) intensity profiles presented as a function of scattering vector (q) for the lamellar EBC/hS blends in which W_S is constant at 0.70 and $w_{S/I}$ is varied: 0.1 (○), 0.2 (●), 0.3 (△) and 0.4 (▲). The data have been shifted vertically to facilitate comparison. The scattering maxima arise from the partially deuterated styrene block in each copolymer, and each peak position (q^*) is related to the lamellar period by Bragg's law ($D = 2\pi/q^*$).

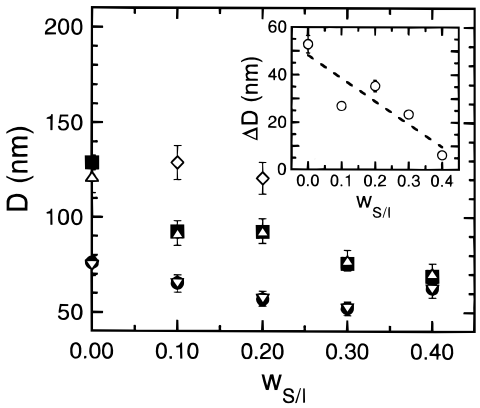

Figure 5. Lamellar period (D) as a function of $w_{S/I}$ for EBC/hS blends, as discerned from SANS (filled symbols) and TEM (open symbols). Blend compositions (in W_S) included here are 0.50 (●, ▽), 0.70 (■, △) and 0.80 (◇). The reduction in D with increasing $w_{S/I}$ reflects intramolecular compatibilization, whereas the coinciding increase in D with increasing W_S is attributed to microdomain swelling. The result of these competitive effects is displayed in the inset, in which the dependence of ΔD (the difference in D evaluated at $W_S = 0.70$ and $W_S = 0.50$) on $w_{S/I}$ is shown. Vertical lines signify the uncertainty in the data (±3% for SANS and ±7% for TEM).

within this copolymer series, the EBCs exhibit lamellar contraction as $w_{S/I}$ is initially increased from 0.0 and approach a lower limit for $w_{S/I} > 0.2$ (equal to ca. 56% of the D evaluated at $w_{S/I} = 0.0$). This trend is likewise observed for the blends with $W_S = 0.70$ (the consistently higher D values reflect the presence of hS). Although no correlation can be discerned from the two lamellar blends with $W_S = 0.80$, they exhibit even larger periodicities due to hS-induced microdomain swelling. Subtraction of the D spacings of the neat copolymers at $W_S = 0.50$ (baseline) from the blends evaluated at $W_S = 0.70$ yields ΔD, a parameter that decouples the relationship between the degrees of hS-induced microstructural swelling and $w_{S/I}$-driven microstructural contraction in the inset of Figure 5. An increase in $w_{S/I}$ lessens the extent to which hS-induced microdomain swelling occurs, with almost no change observed in ΔD for the blend with $w_{S/I} = 0.4$. Since microstructural swelling is maximized if (i) homopolymer molecules localize[26−28,32] near the center of the host block microdomains and (ii) the interfacial regions are relatively narrow and nonobtrusive, ΔD is the greatest for the case of the SI diblock blends. As the interphase is broadened (resulting in an increase in microphase mixing), the effect of hS-induced lamellar swelling decreases, until it is virtually eliminated in the SI40/hS blend.

The reduction in lamellar period upon increasing $w_{S/I}$, along with the more uniformly distributed (less localized) hS within the S-rich microdomains (evidenced by a reduction in the extent of microdomain swelling), is a direct consequence of the random midblock, which serves to make the system less strongly segregated. Inherent in this role of *compatibilizing* attribute is the interpretation of the midblock as a source of intermediate[33] (or delocalized[16]) interactions with hS. Another possible role that the midblock may play in morphological development is that of a nondirectional interfacial rigidifying agent (since it promotes the same outcome in the presence of either added homopolymer). The morphologies evident in Figure 2 for the SI0 diblock represent the established principal morphologies observed in neat block copolymers and their blends. In

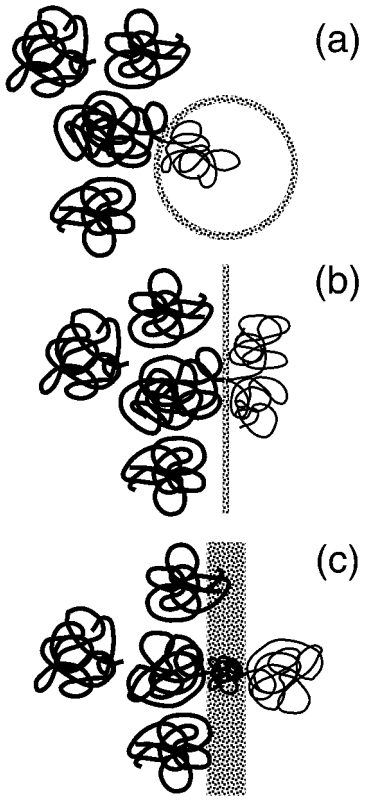

Figure 6. Schematic diagram showing the effect of copolymer molecular architecture on interphase rigidification in the presence of parent homopolymer (hA) molecules at high copolymer dilution. In (a), moderately segregated AB diblock copolymer molecules organize into spherical micelles to minimize repulsive A−B interactions in the presence of hA. If an AB_2 graft copolymer[34,46] is employed (b), packing of the two adjacent B blocks per copolymer molecule serves to stiffen the interphase, resulting in less interfacial curvature than in (a). By extending the interfacial width through the use of an A(A/B)B copolymer (c), the interfacial curvature again decreases relative to (a), and hA molecules are capable of mixing with the broadened interphase due to interaction delocalization.

the case of blends, these transitions reflect changes in interfacial chain packing (and, hence, curvature) as the fraction of homopolymer in the blend is increased (see Figure 6a). By broadening the interphase that separates the S and I microdomains, the amount of hS required to promote a transition necessarily increases. A similar rigidification effect is most likely responsible for the morphologies and stability regimes reported[34] for blends of I_2S graft copolymers with hS. In this case, the presence of two I blocks per S block introduces greater chain-packing constraints on one side of the interphase and hence influences the hS concentration needed to promote a morphological transition (see Figure 6b).[35] Interphase rigidification due to the presence of the random midblock of EBCs is illustrated for comparison in Figure 6c. As mentioned earlier, the transition from lamellae to cylinders is observed in the SI0/hS blend at $W_S = 0.80$ (Figure 2b), whereas the corresponding blends of SI10/hS and SI20/hS at this composition retain swollen lamellar microstructures (Figure 3c,d). The decrease in lamellar swelling for SI30/hS and SI40/hS blends observed in Figure 5, however, indicates that, for $w_{S/I} > 0.2$, the compatibilizing nature of the midblock prevails over the rigidifying effect. This analysis reveals that both the relative midblock length and the blend composition determine

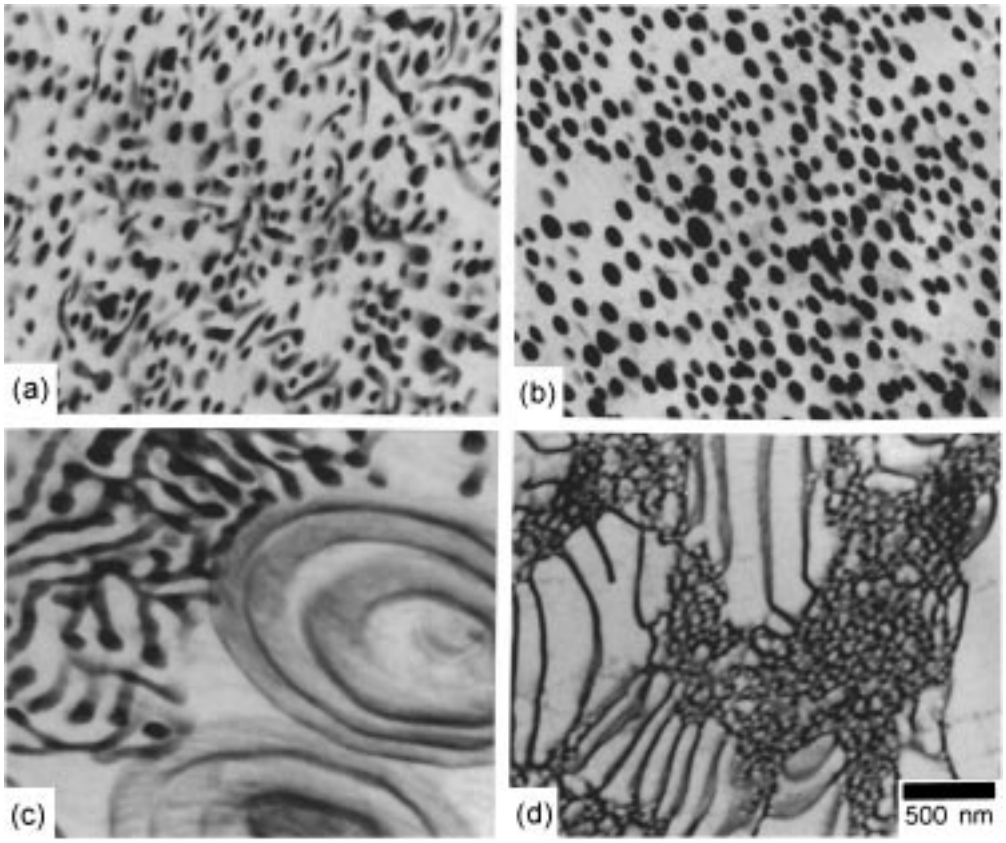

Figure 7. TEM micrographs of EBC/hS blends in which the blend composition is fixed at $W_S = 0.90$ and the copolymer midblock fraction ($w_{S/I}$) is varied: 0.1 (a), 0.2 (b), 0.3 (c), and 0.4 (d). The morphologies observed here parallel those reported and predicted for (co)surfactant solutions: micelles (a, b), coexisting micelles and vesicles (c), and coexisting swollen lamellae and sponge (d).

which midblock role is dominant. Examination of increasingly hS-rich blends reveals that this interplay produces significant morphological variation.

Addition of hS to the copolymers SI10−SI40 at an overall (blend) styrene mass fraction of 0.90 produces the morphological features shown in Figure 7. The SI10/hS blend (Figure 7a) exhibits a dispersed cylindrical morphology that is nearly identical to that of the SI0/hS blend of Figure 2c. Short, stubby cylinders are observed at various orientations with respect to the electron beam, as discussed earlier. A broader size distribution of cylinders is observed for this blend, however, in which the mean diameter ranges from 40 to 50 nm throughout the specimen. As the midblock fraction is doubled, the SI20/hS blend, displayed in Figure 7b, is found to possess isoprene micelles at this composition. These micelles, possessing a mean diameter of 90−95 nm, appear larger than those observed in the micellar SI0/hS blend ($W_S = 0.95$, Figure 2d). This increase in size can be attributed to the increase in molecular weight of the SI20 copolymer relative to that of the SI0 copolymer. Uniaxial alignment of the micelles, a result of section compression during microtomy, is evident in this micrograph.

The SI30/hS and SI40/hS blends in Figure 7c,d ($W_S = 0.90$) exhibit fascinating microstructures similar to those observed in low-molar-mass surfactant systems[36] and in block copolymer/homopolymer ternary blends near the mean-field Lifshitz point.[37,38] It should be recognized, however, that block copolymer molecules self-organize to form a *bilayered* membrane in the present binary blends, but a *monolayered* membrane in ternary blends. Coexisting isoprene micelles and bilayered vesicles form in the SI30/hS blend, whereas coexistence of swollen lamellae with a random self-avoiding bilayered membrane is observed in the SI40/hS blend. The relation of this bilayered structure to the symmetric L_3 (sponge) phase has recently been established.[19] Interestingly, the micellar regions of Figure 7c represent different structures from the spherical micelles of Figure 7b. Isoprene micelles, measuring approximately 40 nm in diameter in this image, clearly show signs of elongation and undulation. Since this deformation occurs isotropically in the micrograph, it is probably not a sectioning artifact. Wormlike micelles have been previously observed in surfactant systems composed of low-molar-mass amphiphilic molecules[39] or short-chain polymers[40] in water or oil. The microstructural elements evident in Figure 7c resemble the isoprene cylinders observed previously but appear to exhibit more flexibility (through bending). A spherical head of larger diameter than the body is also evident for many of the microstructures in Figure 7c, suggesting that these wormlike micelles may constitute a perturbation of spherical micelles (not implying that the head and body possess identical curvatures). In surfactant solutions, wormlike micelles are frequently produced upon the addition of excess salt, which, by screening Coulomb forces, reduces the number of aggregated headgroups per micelle.[41] Lowering the aggregation number destabilizes the spherical structure, and the micelles elongate to compensate. Wormlike micelles have also been observed in I_2S graft copolymers composed of 81 vol % styrene.[34] The chain packing constraints described earlier are believed to be responsible

for observed elongation and curvature variations. In light of these considerations, the formation of wormlike micelles in EBC/hS blends may also constitute an example of interphase rigidification. An alternative explanation for this observed behavior can be derived from comparable phase behavior in low-molar-mass surfactant systems.

The random midblocks of the SI30 and SI40 copolymer molecules are significantly larger than those for copolymers of lower $w_{S/I}$. When $w_{S/I} = 0.3$, the midblock constitutes a source of delocalized attraction and repulsion with the hS matrix.[16] Thus the ability of the midblock to reduce end block segregation behaves in an analogous fashion to excess salt in amphiphilic surfactant solutions; i.e., repulsive interactions between hS and the isoprene end block are effectively "screened" by the midblock. Within the context of this interpretation, the isoprene end block and random midblock of the SI30 and SI40 copolymers can be associated with the headgroup of the corresponding surfactant molecules, while the styrene end blocks act in a manner similar to that of the tails, preferring to associate with the hS matrix rather than with the headgroup. This interpretation is qualitatively consistent with the chemical structure of "extended" surfactants, in which a segment of intermediate polarity is chemically inserted between the head and tail groups.[42]

Having conceptually identified the roles of the EBC blocks in terms of their surfactant nature, we now seek to analyze the progression of copolymer morphologies at a fixed blend composition ($W_S = 0.90$) in Figure 7 from cylinders (SI10) to micelles (SI20), which become wormlike in the presence of bilayered vesicles (SI30) and ultimately form a spongelike microstructure (SI40). Theoretical treatments of surfactant morphologies generally employ interfacial models to account for curvature and elasticity of the surfactant/water (or oil) interface.[41,43−45] On the other hand, prevailing theoretical frameworks addressing block copolymers and their blends in the strong- and intermediate-segregation regimes typically describe the system free energy in terms of a mean potential field and block stretching along the interphase normal in systems exhibiting a microstructure that is well described spatially. Interfacial properties, such as interfacial tension, can then be extracted from such formalisms. An alternative approach, recently proposed by Gido and Wang[46] to predict the preferred interfacial curvature of micellar diblock and graft copolymers, focuses on explicitly describing the interfacial bending (curvature) characteristics of the microstructure. The energy (F) associated with introducing curvature to an interfacial area element dS can generally be written in terms of mean (H) and Gaussian (K) curvatures as[41]

$$F = \int (2\kappa H^2 + \kappa' K)\, \mathrm{d}S \tag{1}$$

where H and K are defined as

$$H = (c_1 + c_2)/2 \tag{2}$$

$$K = c_1 c_2 \tag{3}$$

The principal curvatures c_1 and c_2 are the reciprocals of the principal local curvature radii, R_1 and R_2. The Gaussian curvature is typically used to describe the spatial geometry of a surface: $K > 0$ defines an elliptical surface, $K < 0$ a hyperbolic surface, and $K = 0$ a parabolic surface. Curvature moduli are expressed (on an energy basis) by the mean curvature rigidity (κ) and the Gaussian curvature rigidity (κ'). These parameters represent proportionality constants between interfacial bending and the corresponding change in free energy. Bending the interfacial element dS, for instance, raises F by an amount proportional to κ, whereas the formation of saddle-point (hyperbolic) structures is associated with κ' (which is also referred to as the saddle-splay modulus). Interpretation of morphological characteristics in terms of these moduli also requires definition of the persistence length of the interface (ϵ),[44,45]

$$\epsilon \propto \mathrm{e}^{\kappa/kT} \tag{4}$$

which quantifies the length scale over which fluctuations produce a significant change in curvature. Typical surfactant bilayers have persistence lengths on the order of 100 nm but can be much higher depending on the magnitude of κ.[41]

Formation of wormlike micelles/vesicles in Figure 7c and the sponge phase in Figure 7d both proceed from a perturbation of the swollen lamellar morphology, which ideally possesses two infinite dimensions. Highly correlated (long-wavelength) fluctuations can be supported in lamellar microstructures,[44] producing undulations of the layers on size scales λ greater than ϵ. Unlike short-wavelength fluctuations ($\lambda < \epsilon$), which enhance lamellar stability when $D < \epsilon$,[41] lamellae swollen by solubilized homopolymer become increasingly less stable. For $D \geq \epsilon$, fluctuations of the order $\lambda < \epsilon$ remain stable while those of $\lambda > \epsilon$ induce curvature variations in a manner conceptually similar to a surface random walk.[44] According to de Gennes and Taupin[47] and Cates,[48] the free energy of the system under such conditions is minimized by adopting a different morphology, which may be bicontinuous with a characteristic length scale corresponding to ϵ of the lamellar state and zero mean curvature ($H = 0$). [A minimal surface requires that $H = 0$ and $K < 0$.[49]] The transition of swollen lamellae to either wormlike micelles and vesicles or to the bicontinuous sponge is predicted[44,48,50] to be of first order for surfactant systems. Coexistence of micelles and vesicles in Figure 7c and of swollen lamellae and sponge in Figure 7d supports the assertion that these transitions are also first order for the EBC/hS blends examined here. The analogy proposed earlier, which considers the I end block + S/I midblock as an effective surfactant headgroup attached to a S-end block tail, therefore appears consistent with the observed morphological behavior in dilute EBC/hS blends. In fact, the morphological transitions produced by varying $w_{S/I}$ correspond identically to those predicted and observed in numerous surfactant and cosurfactant solutions. Although detailed analyses[30] of ordered cubic bicontinuous morphologies and cursory observations of a mesh morphology[51] and wormlike micelles[34,46] suggest that long-chain polymer molecules are capable of self-organizing into the entire range of complex (co)surfactant morphologies, the continuous spectrum of micelle-to-sponge transitions has not previously been observed in dilute block copolymer blends. Without the compatibilizing/rigidifying attribute of the random midblock in EBCs, conventional block copolymer blends form cylindrical microdomains in response to large-wavelength fluctuations in the swollen lamellar structure.

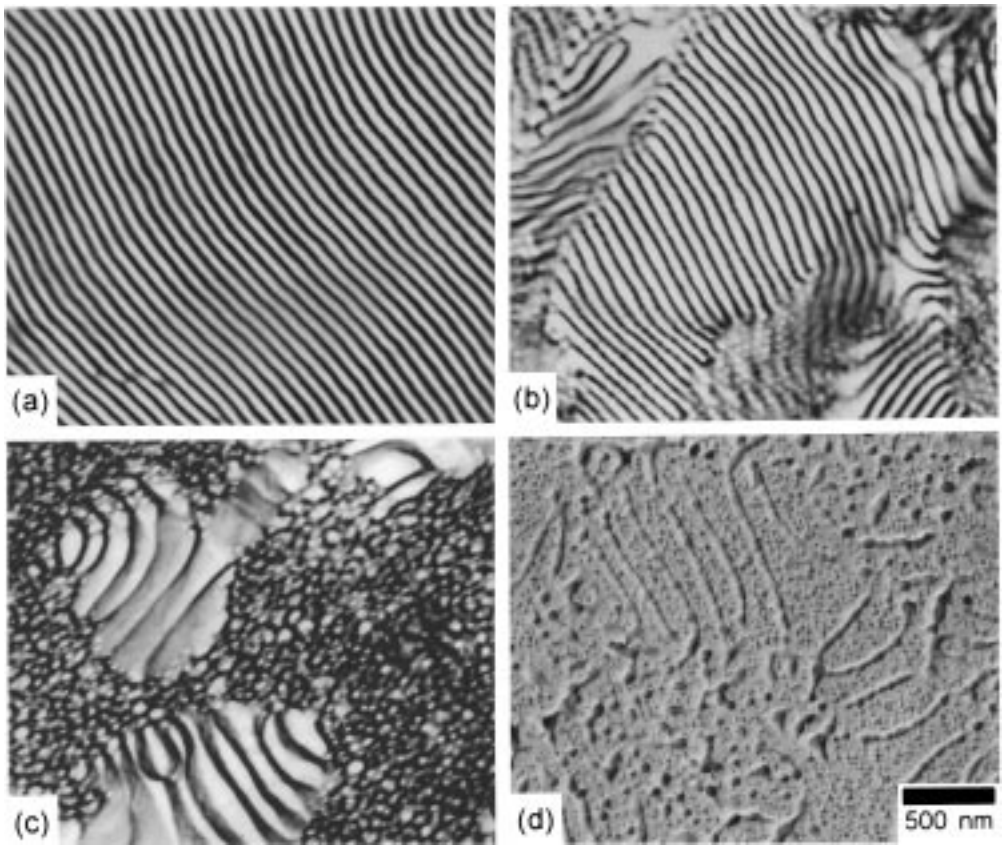

Figure 8. TEM micrographs of SI40/hS blends differing in blend composition (W_S): 0.70 (a), 0.75 (b), and 0.80 (c, d). Highly oriented lamellae are evident in (a), while lamellar grains exhibiting different lamellar orientations, as well as randomly perforated lamellae, are visible in (b). As in Figure 7, coexistence of swollen lamellae and the randomly connected sponge morphology is observed in (c). The cryofracture replica in (d) confirms that the sponge regions in (c) are not the result of an imaging artifact and appears qualitatively similar to cryofracture replicas of sponge-forming (co)surfactant solutions.[54]

To further investigate the first-order transition from swollen lamellae to randomly connected sponge layers, the morphological response of the SI40 copolymer to increasing hS dilution at constant $w_{S/I}$ is presented in the micrographs shown in Figure 8. Under these conditions, lamellar microdomains, such as the ones seen in the blend with $W_S = 0.70$ (Figure 8a) form, with no evidence of vesicles or micelles up to within 5 wt % of the sponge composition (first observed at $W_S = 0.80$). Close examination of the intermediate lamellar composition at $W_S = 0.75$ (Figure 8b) reveals the initial loss of long-range lamellar order. At this composition, the lamellar morphology is characterized by numerous grains exhibiting different periodicities and orientations, as well as the onset of a fine perforated bilayer texture (evidenced by the presence of alternating light/dark circular elements along the bottom portion and left-hand side of Figure 8b). This transition reflects the destabilization of the copolymer lamellae upon hS swelling up to $D \approx \epsilon$. Under these conditions, further microdomain swelling due to additional hS is responsible for the formation of the sponge morphology, as it coexists with swollen lamellae, at $W_S = 0.80$. Note that the micrograph from this blend (Figure 8c) appears nearly identical to that of the blend with $W_S = 0.90$ (Figure 7d).

In light of the randomly perforated lamellar microstructure observed in SI40/hS blends at slightly lower copolymer concentration ($W_S = 0.75$, Figure 8b), steps must be taken to ensure that the sponge morphology is not the (artifactual) result of projection through small, randomly oriented, perforated-lamellar grains. To this end, a detailed three-dimensional reconstruction of the sponge morphology at relatively high spatial resolution has been obtained[19] through the use of transmission electron microtomography. This result reveals, for the first time, real-space information on the randomly connected bilayered membrane inferred[52] from SANS measurements. Examination of a cryofractured replica of the sponge morphology in the SI40/hS blends constitutes an alternative means by which to eliminate section thickness artifacts in projection, while maintaining the characteristics of a direct image. A replica corresponding to the blend featured in Figure 8c is provided in Figure 8d and illustrates the topological features of a *single* fracture plane. Coexisting regions of swollen lamellae and randomly connected channel structures are readily distinguishable, thereby confirming the existence of the sponge morphology. Since previous studies of the sponge morphology have been restricted to low-molar-mass surfactant systems, all existing TEM images of the sponge morphology have been obtained by cryofracture replication.[53,54] Comparison of the replica image in Figure 8d to those obtained by Hoffmann et al.[54] for alkyldimethylamine oxide/heptanol solutions reveals excellent qualitative agreement.[55]

Evidence that the morphological transitions produced in these EBC/hS blends are fundamentally related to those of surfactant systems is also provided in the highly dilute ($W_S = 0.95$) regime. Filali et al.[56] have shown that dilution of the sponge morphology results in the loss of zero mean curvature. Without the low bending energy associated with essentially flat bilayers, the thermodynamically beneficial entropy from the random

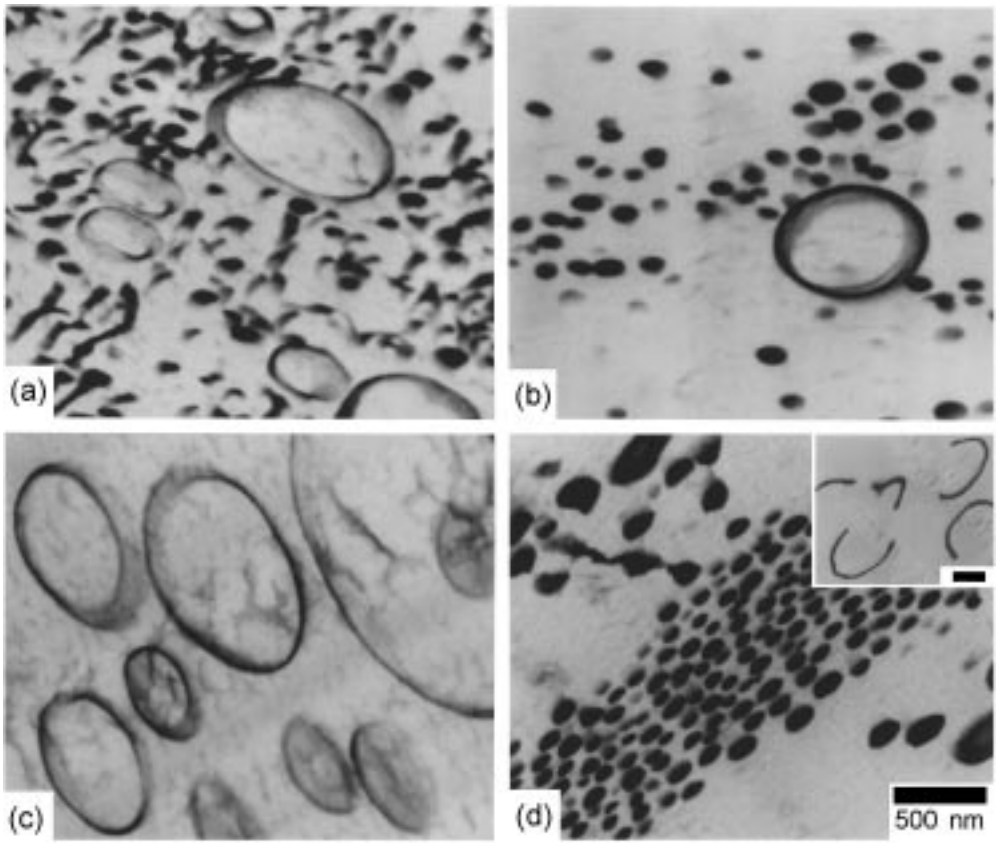

Figure 9. TEM micrographs of the most highly diluted EBC/hS blends examined in this study ($W_S = 0.95$) in which the copolymer midblock fraction ($w_{S/I}$) is varied: 0.1 (a), 0.2 (b), 0.3 (c), and 0.4 (d). Coexisting micelles and unilamellar vesicles are observed for all blends at this concentration. Dissociation of the sponge bilayer in (d) results in the formation of micelles, whereas the swollen lamellae transform into fully formed (albeit not necessarily spherical) vesicles and curved unilamellar sheets.

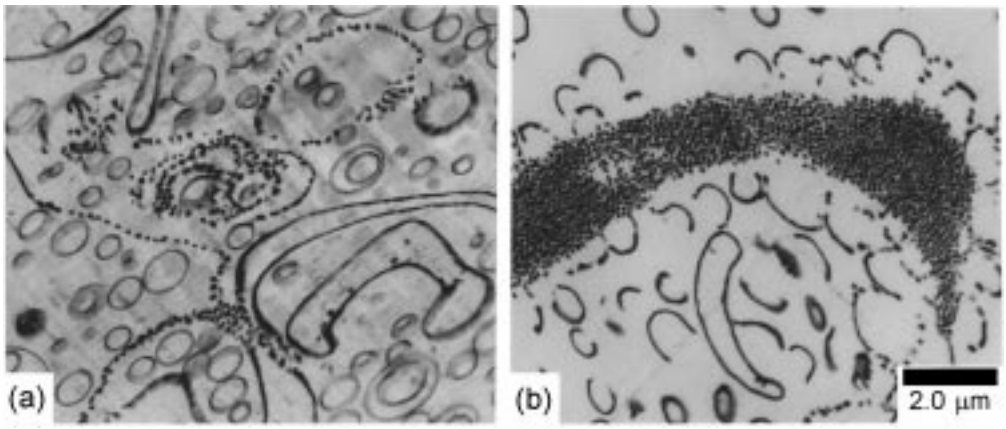

Figure 10. Relatively low-magnification TEM micrographs of the SI30/hS (a) and SI40/hS (b) blends with $W_S = 0.95$. A uniform distribution of micelles and vesicles is observed in (a). The micelles in (b) are associated in regions of comparable size and shape as the sponge regions observed at lower W_S. Note the existence of numerous irregularly shaped vesicles and curved unilamellar sheets in (b).

structure is not sufficient to maintain connectivity of the bilayers. The result is dissociation of the sponge microstructure into vesicles and/or micelles.[41,44,56] A series of EBC/hS blends in which $W_S = 0.95$ is displayed in Figure 9. Copolymers that form cylindrical or micellar morphologies at $W_S = 0.90$ (e.g., SI10 and SI20) are found to self-organize into a micellar + vesicular morphology (Figure 9a,b). Note that this morphology is surprisingly similar to that observed for the SI30/hS blend with $W_S = 0.90$ (Figure 7c). It is interesting that many of the micelles present in the SI10/hS blend (Figure 9a) appear wormlike, while those of the SI20/hS blend (Figure 9b) do not. This feature is consistent with the previous observation that the interfacial rigidifying role of the S/I midblock is pronounced when $w_{S/I} \leq 0.2$. A more rigid interphase would be expected to be less susceptible to the curvature variations associated with wormlike micelles. At higher $w_{S/I}$, unilamellar vesicles are dominant in the SI30/hS blend (Figure 9c), which is seen at low-magnification (Figure 10a) to possess a significantly lower micelle population than the SI30/hS blend with $W_S = 0.90$.

In the case of the sponge morphology, dilution from $W_S = 0.90$ (Figure 7d) to $W_S = 0.95$ (Figure 9d) results in the coexistence of incomplete vesicles (dispersed unilamellar sheets) and micelles, which are consistent

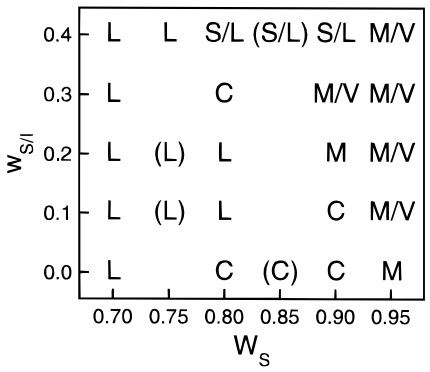

Figure 11. Experimental morphology diagram for the EBC/hS blends examined in this study. Morphologies observed include lamellar (L), cylindrical (C), micellar (M), vesicular (asymmetric L_3) (V), and sponge (symmetric L_3) (S). Coexistence of two morphologies is indicated by the use of two-letter designations. Morphologies shown in parentheses at a given W_S are inferred from the morphologies at higher and lower W_S.

with the surfactant nature of these blends. While these morphological transitions are fundamentally related to those of surfactants, differences exist between Figure 9d and the expected result of diluting the sponge microstructure. In particular, closely packed micelles comprise regions that exhibit the same general size and shape of sponge-rich regions in SI40/hS blends of lower W_S, as seen in the complementary low-magnification image provided in Figure 10b. Dissociation of the sponge microstructure in low-molar-mass surfactant systems is believed[41] to result principally in the formation of bilayered vesicles, rather than micelles, upon further dilution. If the micellar regions in Figures 9d and 10b arise from formerly bicontinuous regions, then it follows that the various sheetlike elements evident in these two images should correspond to the formerly swollen lamellar regions. The abundance of defects in these microstructural elements, such as broken vesicles, certainly supports this viewpoint. Formation of dispersed unilamellar (bilayered) sheets and vesicles adopting noncircular shapes (in projection) reflects, in part, a high interfacial bending energy. This consideration, coupled with the fact that the swollen lamellae in previous micrographs (Figures 7d and 8c) are often interrupted by sponge regions, may explain the preference for micelles, rather than the anticipated vesicles, in this blend.

Conclusions

Chemical incorporation of a random A/B midblock into an AB diblock copolymer has been found to influence significantly the morphological behavior of blends of the resultant copolymers with a parent homopolymer. Four extended block copolymers (EBCs) of the general form A(A/B)B, differing in A/B fraction, as well as the parent diblock copolymer (with no midblock), have been blended with the parent homopolymer A over a broad range of compositions. Morphological characterization of these blends through the use of TEM allows construction of the experimental morphology diagram provided in Figure 11. This diagram summarizes the primary roles of the random midblock in terms of both end block compatibilization and interphase rigidification. While both facets of the midblock role are observed at all blend compositions, interphase rigidification is principally responsible for broadening the lamellar regime in the SI10 and SI20 blends. Compatibilization (i.e., enhanced end block mixing) becomes more prevalent as $w_{S/I}$ increases. Reduction in the lamellar periodicity (measured by both TEM and SANS) confirms that this effect remains significant in the presence of added homopolymer.

The random midblock also serves to delocalize attractive and repulsive interactions with homopolystyrene (hS) when $w_{S/I} \geq 0.3$. This effect has been compared to Coulombic screening in low-molar-mass surfactant systems by virtue of the similarities in morphological development between EBC blends and surfactants at significant levels of dilution. Interaction delocalization also results in a pronounced reduction in lamellar swelling upon addition of hS as $w_{S/I}$ increases, since the hS molecules are no longer thermodynamically restricted to localize near the center of the host block microdomains. When this effect is combined with interphase rigidification, the EBC molecule undergoes morphological transitions analogous to amphiphilic (co)surfactant solutions in water or oil. Nonclassical morphologies, such as wormlike micelles, the asymmetric L_3 (vesicles), and the symmetric L_3 (sponge), have all been observed in these EBC/hS systems. The transitions identified in the $0.90 \leq W_S \leq 0.95$ regime follow those predicted and observed for nonionic surfactants with cosurfactants, as well as ionic surfactants in the presence of excess salt. These transitions have not, to the best of our knowledge, been reported previously for polymer blends. Discovery of such complex microstructures in glassy polymer systems, as opposed to aqueous- or oil-based liquid solutions, provides new and facilitated opportunities for their detailed morphological examination in real space and for their use in applications desiring bilayered, rather than micellar, microstructural elements. Direct three-dimensional imaging of the sponge morphology, for example, has not been previously possible, in which case this fascinating morphology could only be visualized (indirectly) through the use of cryofracture-replication TEM. Emerging microscopy methods not immediately applicable to liquids, such as transmission electron microtomography, may now be applied to a more in-depth analysis of these complex microstructures.

Acknowledgment. We gratefully acknowledge support for this study from the Shell Development Co. and thank A. Ashraf for technical assistance and P. Alexandridis for valuable discussions.

References and Notes

(1) Holden, G.; Legge, N. R.; Quirk, R. P.; Schroeder, H. E. *Thermoplastic Elastomers: A Comprehensive Review*, 2nd ed.; Hanser: New York, 1996.
(2) Park, M.; Harrison, C.; Chaikin, P. M.; Register, R. A.; Adamson, D. H. *Science* **1997**, *276*, 1401. Zhao, D. Y.; Feng, J. L.; Huo, Q. S.; Melosh, N.; Fredrickson, G. H.; Chmelka, B. F.; Stucky, G. D. *Science* **1998**, *279*, 548.
(3) Ruokolainen, J.; Mäkinen, R.; Torkkeli, M.; Mäkelä, T.; Serimaa, R.; ten Brinke, G.; Ikkala, O. *Science* **1998**, *280*, 557.
(4) Bates, F. S.; Fredrickson, G. H. *Annu. Rev. Phys. Chem.* **1990**, *41*, 525.
(5) Leibler, L. *Macromolecules* **1980**, *13*, 1602.
(6) Owens, J. N.; Gancarz, I. S.; Koberstein, J. T.; Russell, T. P. *Macromolecules* **1989**, *22*, 3380.
(7) Bates, F. S.; Schultz, M. F.; Khandpur, A. K.; Förster, S.; Rosedale, J. H.; Almdal, K.; Mortensen, K. *Faraday Discuss.* **1994**, *98*, 7.
(8) Fredrickson, G. H.; Milner, S. T.; Leibler, L. *Macromolecules* **1992**, *25*, 6341.

(9) Galvin, M. E.; Heffner, S.; Winey, K. I. *Macromolecules* **1994**, *27*, 3520. Sikka, M.; Pellegrini, N. N.; Schmitt, E. A.; Winey, K. I. *Macromolecules* **1997**, *30*, 445.
(10) Yerukhimovich, I. Y. *Polym. Sci. U.S.S.R.* **1982**, *24*, 2232.
(11) Annighöfer, F.; Gronski, W. *Colloid Polym. Sci.* **1983**, *261*, 15. Bühler, F.; Gronski, W. *Makromol. Chem.* **1986**, *187*, 2019; **1988**, *188*, 2995.
(12) Tsukahara, Y.; Nakamura, N.; Hashimoto, T.; Kawai, H. *Polym. J.* **1980**, *12*, 455. Hashimoto, T.; Tsukahara, Y.; Tachi, K.; Kawai, H. *Macromolecules* **1983**, *16*, 648.
(13) Kane, L.; Spontak, R. J. *Macromolecules* **1994**, *27*, 1267.
(14) Smith, S. D.; Ashraf, A.; Clarson, S. J. *Polym. Prepr.* **1993**, *34*, 672; **1994**, *35*, 467. Ashraf, A.; Smith, S. D.; Satkowski, M. M.; Spontak, R. J.; Clarson, S. J.; Lipscomb, G. G. *Polym. Prepr.* **1994**, *35*, 581. Smith, S. D.; Ashraf, A.; Satkowski, M. M.; Spontak, R. J. *Polym. Prepr.* **1994**, *35*, 651.
(15) Ashraf, A. M.S. Thesis, University of Cincinnati, 1994.
(16) Laurer, J. H.; Ashraf, A.; Smith, S. D.; Spontak, R. J. *Langmuir* **1997**, *13*, 2250.
(17) Laurer, J. H.; Ashraf, A.; Smith, S. D.; Samseth, J.; Spontak, R. J. *Supramol. Sci.* **1997**, *4*, 121.
(18) Chung, G.-C.; Kornfield, J. A.; Smith, S. D. *Macromolecules* **1994**, *27*, 5729. Chen, Z.-R.; Kornfield, J. A.; Smith, S. D.; Grothaus, J. T.; Satkowski, M. M. *Science* **1997**, *277*, 1248.
(19) Laurer, J. H.; Fung, J. C.; Sedat, J. W.; Smith, S. D.; Samseth, J.; Mortensen, K.; Agard, D. A.; Spontak, R. J. *Langmuir* **1997**, *13*, 2177.
(20) Kim, C.-H.; Park, J.-K.; Hwang, T.-S. *Polym. Eng. Sci.* **1996**, *36*, 535.
(21) Hashimoto, T.; Tanaka, T.; Hasegawa, H. *Macromolecules* **1990**, *23*, 4378. Tanaka, T.; Hasegawa, H.; Hashimoto, T. *Macromolecules* **1991**, *24*, 240.
(22) Winey, K. I.; Thomas, E. L.; Fetters, L. J. *Macromolecules* **1991**, *24*, 6182.
(23) Mayes, A. M.; Russell, T. P.; Satija, S. K.; Majkrzak, C. F. *Macromolecules* **1992**, *25*, 6523.
(24) Spontak, R. J.; Smith, S. D.; Ashraf, A. *Macromolecules* **1993**, *26*, 956.
(25) Winey, K. I.; Thomas, E. L.; Fetters, L. J. *J. Chem. Phys.* **1991**, *95*, 9367. Winey, K. I.; Thomas, E. L.; Fetters, L. J. *Macromolecules* **1992**, *25*, 422, 2645.
(26) Matsen, M. W. *Phys. Rev. Lett.* **1995**, *74*, 4225; *Macromolecules* **1995**, *28*, 8, 5765.
(27) Shull, K. R.; Winey, K. I. *Macromolecules* **1992**, *25*, 2637.
(28) Whitmore, M. D.; Smith, T. W.; *Macromolecules* **1994**, *27*, 4673.
(29) Kinning, D. J.; Thomas, E. L.; Fetters, L. J. *J. Chem. Phys.* **1989**, *90*, 5806.
(30) Hajduk, D. A.; Harper, P. E.; Gruner, S. M.; Honeker, C. C.; Kim, G.; Thomas, E. L.; Fetters, L. J. *Macromolecules* **1994**, *27*, 4063. Laurer, J. H.; Hajduk, D. A.; Fung, J. C.; Sedat, J. W.; Smith, S. D.; Gruner, S. M.; Agard, D. A.; Spontak, R. J. *Macromolecules* **1997**, *30*, 3938. Averopoulos, A.; Dair, B. J.; Hadjichristidis, N.; Thomas, E. L. *Macromolecules* **1997**, *30*, 5634. Sakurai, S.; Irie, H.; Umeda, H.; Nomura, S.; Lee, H. H.; Kim, J. K. *Macromolecules* **1998**, *31*, 336.
(31) Ni, S.; Sakamoto, N.; Hashimoto, T.; Winnik, M. A. *Macromolecules* **1995**, *28*, 8686.
(32) Kimishima, K.; Hashimoto, T.; Han, C. D. *Macromolecules* **1995**, *28*, 3842.
(33) Delocalized interactions may be considered "intermediate" by analogy with the intermediate polarity region in extended surfactants (see ref 41).
(34) Gido, S. P.; Lee, C.; Pochan, D. J.; Pispas, S.; Mays, J. W.; Hadjichristidis, N. *Macromolecules* **1996**, *29*, 7022. Pochan, D. J.; Gido, S. P.; Pispas, S.; Mays, J. W. *Macromolecules* **1996**, *29*, 5099. Pochan, D. J.; Gido, S. P.; Pispas, S.; Mays, J. W.; Ryan, A. J.; Fairclough, J. P. A.; Hamley, I. W.; Terrill, N. J. *Macromolecules* **1996**, *29*, 5091.
(35) Appreciable rigidification of the internal surface of the interphase is not anticipated to occur upon addition of homopolyisoprene, rather than hS, to an I_2S graft copolymer, thereby making this copolymer a "unidirectional" interfacial rigidifying agent.
(36) Hoffmann, H. *Ber. Bunsen-Ges. Phys. Chem.* **1994**, *98*, 1433.
(37) Bates, F. S.; Maurer, W. W.; Lipic, P. M.; Hillmyer, M. A.; Almdal, K.; Mortensen, K.; Fredrickson, G. H.; Lodge, T. P. *Phys. Rev. Lett.* **1997**, *79*, 849. Fredrickson, G. H.; Bates, F. S. *J. Polym. Sci. B: Polym. Phys.* **1997**, *35*, 2775.
(38) Lee, J. H.; Jeon, H. S.; Balsara, N. P.; Newstein, M. C. *J. Chem. Phys.* **1998**, *108*, 5173.
(39) Porte, G.; Appell, J. *J. Phys. Chem.* **1981**, *85*, 2511. Candau, S. J.; Hirsch, E.; Zana, R. *J. Colloid Interface Sci.* **1985**, *105*, 521.
(40) Mortensen, K.; Talmon, Y.; Gao, B.; Kops, J. *Macromolecules* **1997**, *30*, 6764.
(41) Cates, M. E. *Philos. Trans. R. Soc. London A* **1993**, *344*, 339.
(42) Miñana-Perez, M.; Graciaa, A.; Lachaise, J.; Salager, J.-L. *Proc., 4th World Surfactant Congr.* **1996**, *2*, 226.
(43) Porte, G.; Delsanti, M.; Billard, I.; Skouri, M.; Appell, J.; Marignan, J.; Debeauvais, F. *J. Phys. II Fr.* **1991**, *1*, 1101.
(44) Safran, S. A. In *Micelles, Membranes, Microemulsions, and Monolayers*; Gelbar, W. M., Ben-Shaul, A., Roux, D., Eds.; Springer-Verlag: New York, 1994; pp 451−474.
(45) Dan, N.; Safran, S. A. *Macromolecules* **1994**, *27*, 5766.
(46) Gido, S. P.; Wang, Z.-G. *Macromolecules* **1997**, *30*, 6771.
(47) de Gennes, P.-G.; Taupin, C. *J. Phys. Chem.* **1982**, *86*, 2294.
(48) Cates, M. E. *Physica A* **1991**, *176*, 187.
(49) Jinnai, H.; Koga, T.; Nishikawa, Y.; Hashimoto, T. *Phys. Rev. Lett.* **1997**, *78*, 2248. Nishikawa, Y.; Jinnai, H.; Koga, T.; Hashimoto, T.; Hyde, S. T. *Langmuir* **1998**, *14*, 1242.
(50) Roux, D.; Coulon, C.; Cates, M. E. *J. Phys. Chem.* **1992**, *96*, 4174.
(51) Hashimoto, T.; Koizumi, S.; Hasegawa, H.; Izumitani, T.; Hyde, S. T. *Macromolecules* **1992**, *25*, 1433.
(52) Porte, G.; Marignan, J.; Bassereau, P.; May, R. *J. Phys. (Paris)* **1988**, *49*, 511. Marignan, J.; Appell, J.; Bassereau, P.; Porte, G.; May, R. P. *J. Phys. (Paris)* **1989**, *50*, 3553. Hecht, E.; Mortensen, K.; Hoffmann, H. *Macromolecules* **1995**, *28*, 5465.
(53) Jahn, W.; Strey, R. *J. Phys. Chem.* **1988**, *92*, 2294.
(54) Hoffmann, H.; Thunig, C.; Munkert, U.; Meyer, H. W.; Richter, W. *Langmuir* **1992**, *8*, 2629.
(55) Replicas from surfactant systems generally appear to possess sharper features than those from polymeric systems due to differences in material fracture behavior at cryogenic conditions, as well as to the possibility of solvent etching in surfactant systems.
(56) Filali, M.; Porte, G.; Appell, J.; Pfeuty, P. *J. Phys. II Fr.* **1994**, *4*, 349.

MA980200J